Letter

How flagellated bacteria wobble

Chen Gui,[1,*] Mingxin Mao,[1,2,*,†] Pu Feng,[3,*] Yuxin Shen,[3] Xiangjun Gong,[3,‡] Gerhard Gompper,[4,§] and Jinglei Hu[1,‖]

[1]*Kuang Yaming Honors School, Nanjing University, Nanjing 210023, China*
[2]*Department of Physics, Tsinghua University, Beijing 100084, China*
[3]*Faculty of Materials Science and Engineering, South China University of Technology, Guangzhou 510640, China*
[4]*Theoretical Physics of Living Matter, Institute for Advanced Simulation, Research Center Jülich, 52425 Jülich, Germany*

(Received 3 July 2024; accepted 5 December 2025; published 28 January 2026; corrected 10 March 2026)

The wobbling motion of flagellated bacteria significantly influences their swimming behavior, yet its dynamics remains poorly understood, primarily due to the difficulty in tracking the 3D orientations of both the flagellar bundle and the cell body. Here, we use hydrodynamics simulations of a mechanical *Escherichia coli* model in polymer fluids with varying wobbling amplitudes and flagellar anchoring configurations to elucidate this motion. Through Euler angle analysis, we resolve the three components of wobbling: precession, nutation, and spin. Our findings challenge the common assumption that peritrichous bacteria undergo complete cycles of body spin. Notably, we uncover a small-amplitude nutation with a well-defined period on the order of a few milliseconds. We also identify two distinct precession modes. To interpret these findings, we develop a theoretical framework based on Lagrangian mechanics.

DOI: 10.1103/g3w4-5jw8

Introduction. As one of the oldest living forms on Earth and a unique kind of active colloids, bacteria now are also studied as models for nonequilibrium systems and motile active matter. Peritrichous bacteria such as *Escherichia coli* exploit a bundle of multiple helical flagella for locomotion [1]. Numerous studies have been performed to unravel the swimming behavior of single *E. coli* or other flagellated bacteria in bulk [2–9] or near surfaces [10–17], as well as the collective behavior of bacterial swarms [18–20]. The wobbling motion of the cell body around its swimming direction was initially visualized for *E. coli* [2] and has been experimentally shown to profoundly affect the bacterial swimming behavior. For instance, wobbling induces helical swimming paths for *Bacillus subtilis* [21], *Caulobacter crescentus* [5], and *Helicobacter pylori* [22]. The suppression of wobbling contributes to the enhanced swimming speed of *E. coli* in complex fluids [7,9]. However, the kinematics and dynamics of bacterial wobbling remain elusive.

The wobbling motion detected in experiments [2,5,21–23] reflects the precession of the bacterial body that has an off-axis orientation with respect to the counterrotating flagellar bundle. As a rotating rigid body, the bacterial body might nutate while precessing. This naturally leads to fundamental questions, like: How does the bacterium precess, with one direction or with two alternating directions? Does the bacterium exhibit periodic nutation? If so, what is the rate of nutation compared to precession?

Our comprehension of the bacterial wobbling kinematics and dynamics is limited by experimental challenges in tracking the 3D orientations of the body and the flagellar bundle. Phase-contrast microscopy [2,22,24] offers direct 2D images of the whole bacterium, while digital holography [5,14,16,25,26] provides 3D trajectories of bacterial swimming across a large volume by reconstructing the coordinates of the cell body's centroid. Though apparent wobbling periods can be derived from these images and trajectories, discerning wobbling kinematics—such as precession mode, nutation, and spin—requires knowledge of orientations of both the body and the flagellar bundle, as will become evident through our detailed analysis below, which is not accessible experimentally. From a theoretical standpoint, the friction between the cell body and the multiple flagella as well as near-field hydrodynamics [6] pose substantial challenges for an analytical description of the wobbling of peritrichous bacteria.

In this Letter, we overcome the experimental and analytical limitations by performing extensive hydrodynamics simulations of a quantitative mechanical model [6,15,27] of *E. coli* with different wobbling amplitudes and flagellar anchoring configurations. The wobbling amplitude is defined by the angle between the flagellar bundle and the body, and is systematically varied by introducing polymer chains in solution that exhibit steric repulsion with the bacterium [28]. By tracking the orientations of both the body and the flagellar bundle, we perform Euler angle analysis, which enables us to quantify the three components underlying the apparent wobbling: precession, nutation, and spin. Our simulations reveal a surprising finding that the cell body does not undergo full

*These authors contributed equally to this work.
†Contact author: maomx25@mails.tsinghua.edu.cn
‡Contact author: msxjgong@scut.edu.cn
§Contact author: g.gompper@fz-juelich.de
‖Contact author: hujinglei@nju.edu.cn

Published by the American Physical Society under the terms of the Creative Commons Attribution 4.0 International license. Further distribution of this work must maintain attribution to the author(s) and the published article's title, journal citation, and DOI.

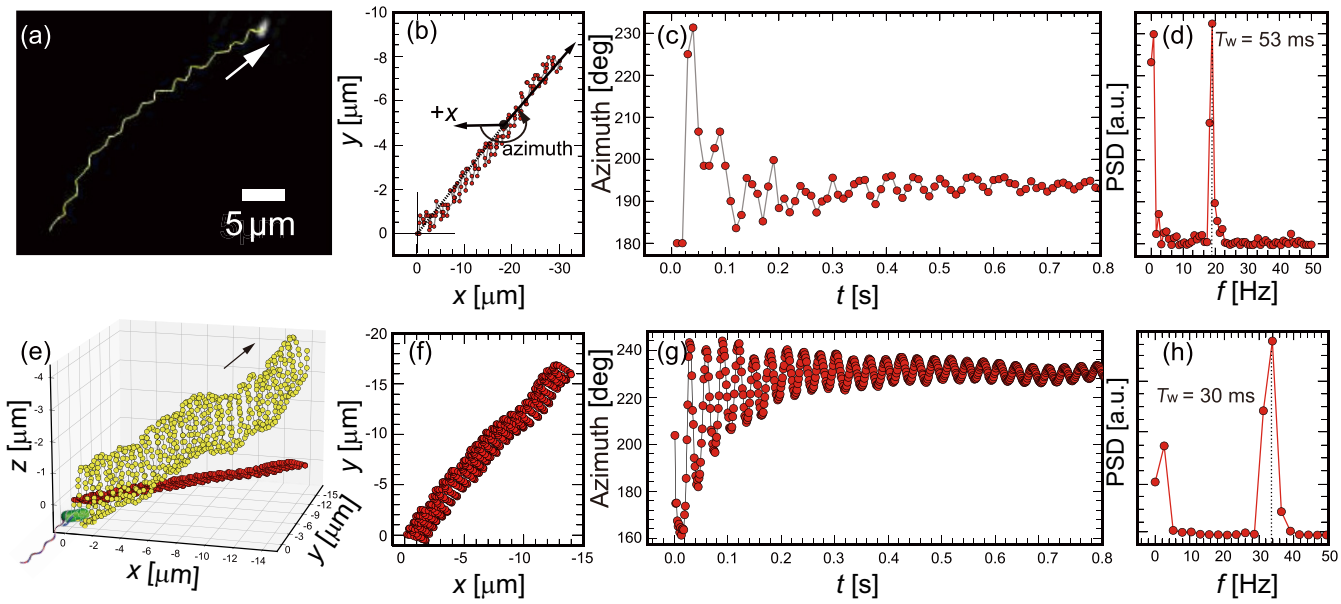

FIG. 1. Analysis of *E. coli* wobbling in water using experimental [panels (a)–(d)] and simulated [panels (e)–(h)] swimming trajectories. (a) 2D swimming trajectory with the arrow indicating the swimming direction. (b) 2D trajectory displayed in the xy plane, where each point defines an azimuth angle $\pi + \arctan(y/x)$. (c) Time series of the azimuth for the trajectory in panel (b). Only the initial part is shown here for better visualization of the oscillation. (d) Power spectrum of the azimuth in panel (c). (e) 3D helical trajectory of a tracer particle located at one pole of the cell body from hydrodynamics simulations. The red trajectory is a 2D projection in the xy plane. Panels (f)–(h) are derived from the trajectory in panel (e).

cycles of spin, contrary to the common view. Remarkably, we discover a high-frequency nutation with a period on the order of a few milliseconds, which is attributed to repeated collisions between the rotating flagella and cell body. Additionally, we observe two types of precession modes. To interpret these previously unreported findings, we develop a theoretical framework based on Lagrangian mechanics.

Results and discussion. Figure 1(a) shows a 2D swimming trajectory of *E. coli* in water obtained using digital holographic microscopy (see the Supplemental Material [29]). To measure the apparent wobbling period, we define the azimuth angle between $+x$ axis and the unit vector $\mathbf{u}$ pointing from the initial position to each coordinate along the trajectory [Fig. 1(b)]. The oscillations of this azimuth angle [Fig. 1(c)] reflect the body's wobbling evident in the trajectory. When the bacterium is near the initial position, a small change in y coordinate can cause a large change in $\mathbf{u}$, leading to strong oscillations of azimuth. As the bacterium swims farther from its initial position, the same change in y coordinate results in only minor variations in $\mathbf{u}$, leading to smaller oscillations. The power spectrum of the azimuth [Fig. 1(d)] exhibits a primary peak with the wobbling period of $T_w = 53$ ms, close to Darnton *et al.*'s experimental result of 80 ms [2]. Simulation results for our model *E. coli* (text and Fig. S1 in the Supplemental Material [29]), with four asymmetrically distributed flagellar anchors and swimming in water, are displayed in Figs. 1(e)–1(h). The 3D yellow trajectory of a tracer bead at one pole of the body [Fig. 1(e)] illustrates a helical swimming path as observed for many flagellated bacteria [5,21,22]; see Table S1 in the Supplemental Material [29] for the pitch and radius of each simulated trajectory. The 2D projection of the helical trajectory, using the same procedure as for the experimental data in Figs. 1(b)–1(d), yields $T_w = 30$ ms [Fig. 1(h)], in reasonable agreement with the experimental result of $T_w = 53$ ms. This validates both our hydrodynamics simulations and the protocol used to extract T_w from 2D trajectories. As will be shown below, T_w corresponds to the precession period T_P.

We proceed with the detailed analysis of the wobbling based on simulations. As shown in Fig. 2(a), since the precession and nutation of the spherocylindrical body or the helical flagellar bundle cause the reorientation of its axis ($\mathbf{e}_3$ or $\mathbf{e}_f$), these two kinds of motions can be visualized by tracking the trajectory of one end of the axis on the surface of a unit sphere, while fixing the other end at the sphere's center. Figure 2(b) provides a top view of the initial four cycles of the trajectories swept by $\mathbf{e}_3$ (in red) and $\mathbf{e}_f$ (in blue). The trajectories are not drawn to scale for clarity. Both the body and flagellar bundle precess counterclockwise [46] and complete nearly an equal number of cycles within the same time frame, implying synchronization in their precession. This finding explains the experimental observation that the orientation of *Helicobacter pylori*'s flagellar bundle changes with respect to the body [22]. The nutation of the body and flagellar bundle becomes apparent starting from the third cycle and is also synchronized, as evidenced by the concurrent emergence of distinct "kinks" in the trajectories. One cycle of accurately scaled trajectories in the steady state is provided in the rightmost panel of Fig. 2(b), each comprising 32 points with a total duration of 46.5 ms. There are six "kinks" in the single cycle of each trajectory, indicating that the precession period T_P is about 6 times the nutation period T_N. We then have the estimates $T_P \approx 46.5$ ms

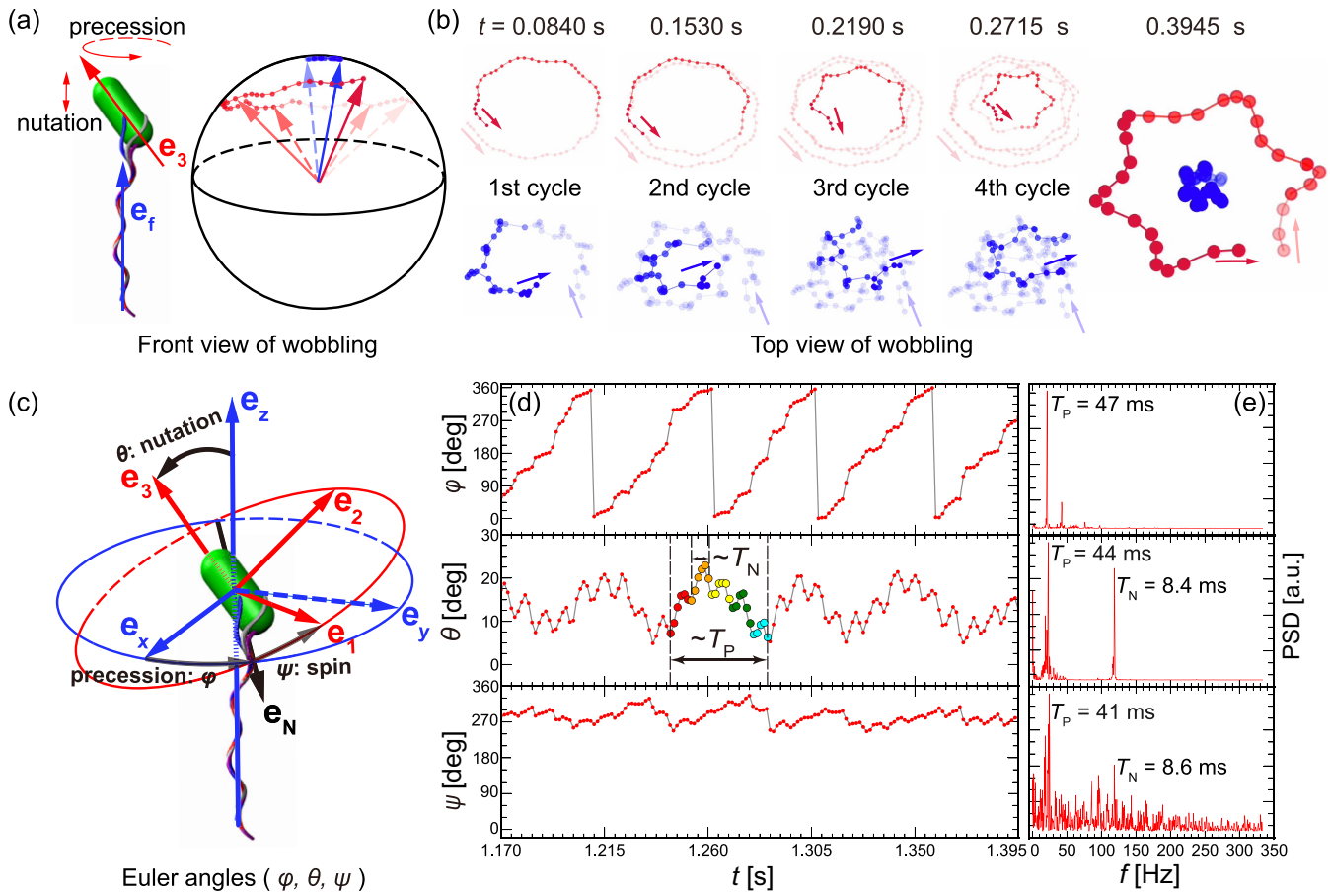

FIG. 2. Kinematic analysis of the wobbling of simulated *E. coli* with asymmetric flagellar anchors in polymer solution with concentration $c = 0.20$. (a) Front view of the wobbling. The precession and nutation of the spherocylindrical body or the helical flagellar bundle are tracked *via* the trajectory of one end of its axis ($\mathbf{e}_3$ or $\mathbf{e}_f$) on a unit sphere's surface, with the other end fixed at the sphere's center. (b) The initial four cycles of trajectories traced by $\mathbf{e}_3$ (in red) and $\mathbf{e}_f$ (in blue) are depicted in a top view, although not drawn to scale for clarity. Both the body and the flagellar bundle precess counterclockwise. Trajectories in the rightmost panel are accurately scaled. (c) Two coordinate systems defined by the orthogonal bases ($\mathbf{e}_x, \mathbf{e}_y, \mathbf{e}_z$) and ($\mathbf{e}_1, \mathbf{e}_2, \mathbf{e}_3$) are used to derive the Euler angles (φ, θ, ψ) that quantify the precession, nutation, and spin of the body. See the main text for details. (d) Time series of the Euler angles extracted from the simulation data. (e) Power spectra of the angles in panel (d).

and $T_N \approx 7.75$ ms. The observation that $\mathbf{e}_3$ traces a much larger cycle than $\mathbf{e}_f$ justifies to regard $\mathbf{e}_f$ as the precession axis $\mathbf{e}_z$ of the body for kinematic analysis.

To quantify the wobbling kinematics, we extract the Euler angles of the bacterial body from its long axis $\mathbf{e}_3$ and the flagellar bundle's axis $\mathbf{e}_z$ monitored throughout the simulations [47]. It remains a challenge to acquire the two axes from laboratory experiments. Two coordinate systems are used to derive the Euler angles φ, θ, and ψ for the description of precession, nutation, and spin of the body, as shown in Fig. 2(c). The flagellar bundle determines the reference coordinate system ($\mathbf{e}_x, \mathbf{e}_y, \mathbf{e}_z$), whereas the other basis ($\mathbf{e}_1, \mathbf{e}_2, \mathbf{e}_3$) specifies the body-fixed coordinate system. $\mathbf{e}_N$ defines intersection line of the $\mathbf{e}_x$-$\mathbf{e}_y$ and $\mathbf{e}_1$-$\mathbf{e}_2$ planes. φ is then defined by $\mathbf{e}_x$ and $\mathbf{e}_N$, θ by $\mathbf{e}_z$ and $\mathbf{e}_3$, and ψ by $\mathbf{e}_N$ and $\mathbf{e}_1$. The time series of the three angles in Fig. 2(d) exhibits periodic variations. Surprisingly, the spin angle ψ fluctuates within a narrow range instead of varying monotonically between 0° and 360°, indicating that the body undergoes slight back-and-forth rotation around $\mathbf{e}_3$ without a distinct direction. This finding is further supported by the unnoticeable change in the tracer's position relative to the body's axis during precession [Fig. S2(a) in the Supplemental Material [29]] and contradicts the common assumption that the bacterial body in general rotates around its own axis in the opposite direction to the rotation of the flagellar bundle. For peritrichous bacteria, the body and the flagellar bundle precess simultaneously through constant adjustments of each flagellum's anterior part (Movie S1 in the Supplemental Material [29]). However, complete cycles of body spin, which would cause continuous twisting and stretching of each flagellum, are physically impossible [48]. Conversely, the flagellar bundle spins in the opposite direction to the precession at a rate about 5 times faster than the precession [Figs. S2(b)–S2(d) and text in the Supplemental Material [29]]. Neither the distinction between the body's precession and spin nor the absence of complete body spin has been reported in previous studies of bacterial motion. To account for the counterrotation of bacterial body and flagella [6,15], the rotlet dipole has been incorporated into simplified hydrodynamic models of bacteria. Since precession and nutation also contribute to the

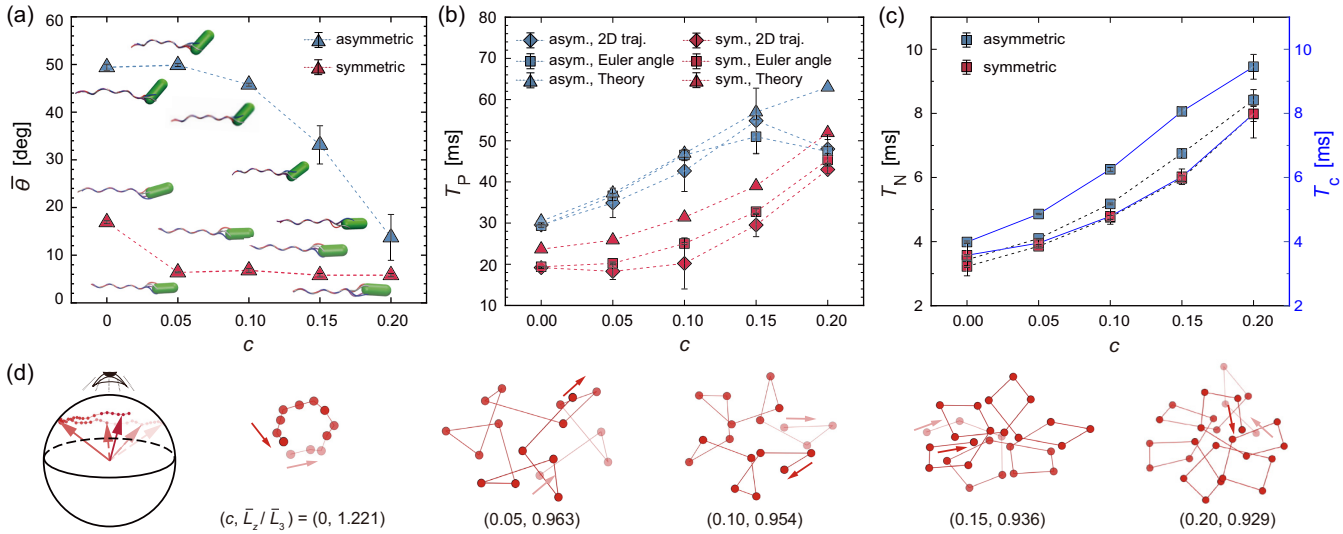

FIG. 3. Precession and nutation of *E. coli* in polymer solution with varying wobbling amplitudes and flagellar anchoring. (a) Wobbling amplitude, defined by the average nutation angle $\bar{\theta}$, is tuned by concentration c of added polymers. Inserted are snapshots of each bacterium. (b) Period of precession T_P *vs* c, as derived from 2D trajectories, Euler angles, and theory (see the Supplemental Material [29]). (c) Period of nutation T_N and period of flagellum-body collision T_c *vs* c. T_N is extracted from Euler angle θ. (d) Trajectories similar to Fig. 2(b) but for *E. coli* with symmetric flagellar anchors. The last four trajectories are zoomed in 4× to better visualize the precession with alternating directions. At each value of c, the ratio $\bar{L}_z/\bar{L}_3$ is determined from simulation averages.

overall rotation of both the cell body and flagella, the lack of body spin in peritrichous bacteria does not call into question the applicability of the rotlet dipole approximation.

The power spectra in Fig. 2(e) for the Euler angles unveil the periods of the underlying motions. The upper panel for the precession angle φ reveals a period of $T_P = 47$ ms, consistent with the estimate of $T_P \approx 46.5$ ms from visual inspection of the trajectories in the rightmost panel of Fig. 2(b) and the apparent wobbling period $T_w = 48$ ms derived from the 2D swimming trajectory (Fig. S3 in the Supplemental Material [29]). The middle panel for the nutation angle θ exhibits a secondary peak with a period of $T_N = 8.4$ ms, in accord with the previous estimate of nutation period $T_N \approx 7.75$ ms. This signal of nutation period clearly shows that the nutation is driven by an active torque instead of thermal noise. A closer look at the time series of θ in Fig. 2(d) reveals that one precession cycle roughly consists of 29 points, with a total duration of 42 ms. The high-frequency periodic fluctuations of about 5° around the local average of θ, as depicted by the five groups of points in different colors, mirror the body's small-amplitude nutation. The estimated nutation amplitude for each *E. coli* is listed in Table S1 in the Supplemental Material [29]. Such nutation is hardly detectable from power spectral analysis of the 2D swimming trajectory with high spatial and temporal resolutions (text and Fig. S3 in the Supplemental Material [29]). Experimental measurement of the nutation therefore must be exceedingly difficult. The quantitative agreement between the power spectral analysis and the visual inspection of both the simulated time series and the trajectories in Fig. 2 confirms the reliability of our approach for quantifying the precession and nutation using Euler angles. The emergence of the precession signal ($T_P = 44$ ms) in the power spectrum of the nutation angle θ and the emergence of precession ($T_P = 41$ ms) and nutation ($T_N = 8.6$ ms) signals in the power spectrum of the spin angle ψ are explained in the Supplemental Material [29].

The wobbling dynamics can be modified by introducing soluble polymers into the embedding fluid. As shown in Fig. 3(a), the average nutation angle $\bar{\theta}$ decreases with increasing polymer concentration c, consistent with experimental observations in Ref. [7]. This reduction arises because steric repulsion between the bacterium and added polymers acts against the elastic deformations of each flagellum, thereby suppressing the wobbling amplitude. Figure 3(b) further shows that the precession period T_P increases with c, primarily due to the slowdown of rotations caused by increased fluid viscosity [Fig. S1(b) in the Supplemental Material [29]]. Our experiments confirm the same trend (Fig. S4 in the Supplemental Material [29]). Moreover, the values of T_P extracted from the 2D swimming trajectories and from Euler angles agree with those predicted from our theory based on Lagrangian mechanics [Eq. (S17) and text in the Supplemental Material [29]]. This agreement highlights two key effects of polymer addition captured by Eq. (S17) in the Supplemental Material [29]: (1) reduction of $\bar{\theta}$ due to bacterium-polymer repulsion and (2) increased fluid viscosity, which lowers both the bacterial swimming speed v_z [Fig. S1(b) in the Supplemental Material [29]] and flagellar angular speed ω_f [Fig. S2(d) in the Supplemental Material [29]].

Figure 3(c) shows that the nutation period T_N is much shorter than the precession period T_P. According to the dynamical equation for nutation, Eq. (S9) in the Supplemental Material [29], a periodic torque is required to drive the body's rhythmic nutation. Thermal fluctuations induce variations in the nutation angle θ, and the flagellar elastic deformations in response to these variations act to restore the angle, leading

to aperiodic fluctuations in θ that complicate the detection of nutation. Without an active torque matching the nutation period T_N, the body would not exhibit periodic changes in θ, as the bacterial motion is overdamped. A plausible source of this active torque is the flagellum-body collision [6]. As each flagellum rotates under motor torque and constantly adjusts the spatial arrangement of its unbundled anterior segment to maintain counterrotation between the body (angular speed ω_b) and flagellar bundle (ω_f), it frequently collides with the body. These repeated collisions, occurring with a period $T_c \approx 2\pi/(\omega_f + \omega_b)$, are supposed to generate the active torque. This hypothesis is supported by the quantitative agreement between T_N and T_c shown in Fig. 3(c). Taken together, the repeated collisions between the rotating flagella and cell body are responsible for the nutation.

Now we discuss how the flagellar number, length, and anchoring positions influence the nutation period by analyzing their effects on ω_f and ω_b. Since multiple flagella, anchored at different sites on the body, form a helical bundle that propels the bacterium, the flagellar number and positioning dictate (1) the tilt of the bundle relative to the long axis of the spherocylindrical body, characterized by the angle θ, and (2) the flagellum-body and flagellum-flagellum friction. Assuming a constant motor torque per flagellum, these factors determine the effective torque rotating the flagellar bundle τ_f, as well as the opposite torque rotating the body, which typically represents only a fraction of the total motor torque due to friction [6]. The flagellar length generally does not affect τ_f or θ. Equations (S17) and (S19) in the Supplemental Material [29] show that ω_f depends on the flagellar length in a nontrivial fashion. Given τ_f and θ, ω_f and ω_b can be estimated according to Eqs. (S19) and (S20) in the Supplemental Material [29]. However, accurate modeling of τ_f is challenging due to the intricate flagellum-body friction and near-field hydrodynamics. Nevertheless, Fig. 3(c) shows that the nutation period is surprisingly insensitive to whether the four flagella are symmetrically or asymmetrically anchored to the cell body.

Figure 3(d) illustrates the two distinct precession modes observed in *E. coli* with symmetric flagellar anchors. In water ($c = 0$), the cell body exhibits normal precession with counterclockwise direction when viewed from the top. In polymer solutions ($c = 0.05$–0.20), the body precesses with alternating directions, i.e., short-term clockwise and long-term counterclockwise. These two modes can be understood by considering the two components of the angular momentum $\mathbf{L}$ of the body, $L_3 = \mathbf{L}\cdot\mathbf{e}_3 = I_3(\dot{\psi} + \dot{\varphi}\cos\theta)$ and $L_z = \mathbf{L}\cdot\mathbf{e}_z = (I_1\sin^2\theta + I_3\cos^2\theta)\dot{\varphi} + I_3\dot{\psi}\cos\theta$, which can be regarded in the steady state as constant quantities [49]. Here, I_1 and I_3 are the moments of inertia of the spherocylindrical body along $\mathbf{e}_1$ and $\mathbf{e}_3$, and include the effect of hydrodynamic friction. The stronger the friction, the smaller I_1 and I_3. The precession angular velocity is then

$$\dot{\varphi} = (L_z - L_3\cos\theta)/I_1\sin^2\theta, \tag{1}$$

which implies that normal precession ($\dot{\varphi} > 0$) occurs when $L_z > L_3$. When $L_z < L_3$, there exists a value of θ at which $\dot{\varphi} = 0$. In this case, precession with alternating directions occurs. Since the cell body does not spin, i.e., $\dot{\psi} \approx 0$, the condition $L_z < L_3$ reduces to $I_3/I_1 > \sin^2\theta/(\cos\theta - \cos^2\theta)$. The two precession modes of *E. coli* discovered in our simulations perfectly match the predictions from Eq. (1) (Fig. S5 in the Supplemental Material [29]). Our findings demonstrate that steric repellant can be used to regulate bacterial precession and that flagellated bacteria with small nutation angles and large body aspect ratios (i.e., large I_3/I_1) preferentially adopt the precession mode with alternating directions.

Conclusions. We have investigated the wobbling dynamics of flagellated bacteria by combining simulations, theory, and experiments. Our findings of the absence of full body spin, periodic nutation, and two distinct precession modes enrich the physical picture of bacterial motion. These results provide insights into bacterial dynamics and contribute to the broader understanding of nonequilibrium physics in active matter systems.

Our findings further reveal important biological implications. In environmental and biological fluids, where polymers are ubiquitous, steric interactions strongly modulate bacterial wobbling. Such polymer-induced regulation of motion may represent a general mechanism that shapes how bacteria explore complex habitats and interact with mucosal layers.

Acknowledgments. J.H. thanks the National Natural Science Foundation of China (Grants No. 22473058 and No. 12232019) and the Key Project of the Ministry of Education's Top-notch Students Training Program 2.0 for Basic Disciplines (Grant No. 20251014). X.G. acknowledges support from the National Key R&D Program of China (Grant No. 2024YFA0920100), Guangdong Basic and Applied Basic Research Foundation (Grant No. 2024A1515011926), Guangdong Key-Area R&D Program (Grant No. 2023B0101200006), and the State Key Laboratory of Applied Microbiology Southern China (Grant No. SKLAM008-2022). C.G. appreciates discussions with Mr. Yurui Liu. All simulations were performed at Nanjing University's High Performance Computing Center.

Data Availability. The data that support the findings of this article are openly available [47].

[1] H. C. Berg, *E. Coli in Motion* (Springer, New York, 2004).

[2] N. C. Darnton, L. Turner, S. Rojevsky, and H. C. Berg, On torque and tumbling in swimming *Escherichia coli*, J. Bacteriol. **189**, 1756 (2007).

[3] N. Watari and R. G. Larson, Swimming hydrodynamics of a run-and-tumble bacterium with helical flagella, Biophys. J. **98**, 160A (2010).

[4] V. A. Martinez, J. Schwarz-Linek, M. Reufer, L. G. Wilson, A. N. Morozov, and W. C. K. Poon, Flagellated bacterial motility in polymer solutions, Proc. Natl. Acad. Sci. USA **111**, 17771 (2014).

[5] B. Liu, M. Gulino, M. Morse, J. X. Tang, T. R. Powers, and K. S. Breuer, Helical motion of the cell body enhances *Caulobacter crescentus* motility, Proc. Natl. Acad. Sci. USA **111**, 11252 (2014).

[6] J. Hu, M. Yang, G. Gompper, and R. G. Winkler, Modelling the mechanics and hydrodynamics of swimming *E. coli*, Soft Matter **11**, 7867 (2015).

[7] A. E. Patteson, A. Gopinath, M. Goulian, and P. E. Arratia, Running and tumbling with *E. coli* in polymeric solutions, Sci. Rep. **5**, 15761 (2015).

[8] A. Zöttl and J. M. Yeomans, Enhanced bacterial swimming speeds in macromolecular polymer solutions, Nat. Phys. **15**, 554 (2019).

[9] S. Kamdar, S. Shin, P. Leishangthem, L. F. Francis, X. Xu, and X. Cheng, The colloidal nature of complex fluids enhances bacterial motility, Nature (London) **603**, 819 (2022).

[10] W. R. DiLuzio, L. Turner, M. Mayer, P. Garstecki, D. B. Weibel, H. C. Berg, and G. M. Whitesides, *Escherichia coli* swim on the right-hand side, Nature (London) **435**, 1271 (2005).

[11] E. Lauga, W. R. DiLuzio, G. M. Whitesides, and H. A. Stone, Swimming in circles: Motion of bacteria near solid boundaries, Biophys. J. **90**, 400 (2006).

[12] A. P. Berke, L. Turner, H. C. Berg, and E. Lauga, Hydrodynamic attraction of swimming microorganisms by surfaces, Phys. Rev. Lett. **101**, 038102 (2008).

[13] R. Di Leonardo, D. Dell'Arciprete, L. Angelani, and V. Iebba, Swimming with an image, Phys. Rev. Lett. **106**, 038101 (2011).

[14] M. Molaei, M. Barry, R. Stocker, and J. Sheng, Failed escape: Solid surfaces prevent tumbling of *Escherichia coli*, Phys. Rev. Lett. **113**, 068103 (2014).

[15] J. Hu, A. Wysocki, R. G. Winkler, and G. Gompper, Physical sensing of surface properties by microswimmers—Directing bacterial motion via wall slip, Sci. Rep. **5**, 9586 (2015).

[16] S. Bianchi, F. Saglimbeni, and R. Di Leonardo, Holographic imaging reveals the mechanism of wall entrapment in swimming bacteria, Phys. Rev. X **7**, 011010 (2017).

[17] D. Cao, M. Dvoriashyna, S. Liu, E. Lauga, and Y. Wu, Reduced surface accumulation of swimming bacteria in viscoelastic polymer fluids, Proc. Natl. Acad. Sci. USA **119**, e2212078119 (2022).

[18] X. Chen, X. Dong, A. Be'er, H. L. Swinney, and H. P. Zhang, Scale-invariant correlations in dynamic bacterial clusters, Phys. Rev. Lett. **108**, 148101 (2012).

[19] C. Chen, S. Liu, X.-Q. Shi, H. Chaté, and Y. Wu, Weak synchronization and large-scale collective oscillation in dense bacterial suspensions, Nature (London) **542**, 210 (2017).

[20] S. Liu, S. Shankar, M. C. Marchetti, and Y. Wu, Viscoelastic control of spatiotemporal order in bacterial active matter, Nature (London) **590**, 80 (2021).

[21] Y. Hyon, Marcos, T. R. Powers, R. Stocker, and H. C. Fu, The wiggling trajectories of bacteria, J. Fluid Mech. **705**, 58 (2012).

[22] M. A. Constantino, M. Jabbarzadeh, H. C. Fu, and R. Bansil, Helical and rod-shaped bacteria swim in helical trajectories with little additional propulsion from helical shape, Sci. Adv. **2**, e1601661 (2016).

[23] S. Bianchi, F. Saglimbeni, A. Lepore, and R. Di Leonardo, Polar features in the flagellar propulsion of *E. coli* bacteria, Phys. Rev. E **91**, 062705 (2015).

[24] H. Zheng, N. Yan, W. Feng, Y. Liu, H. Luo, and G. Jing, Swimming of buoyant bacteria in quiescent medium and shear flows, Langmuir **39**, 4224 (2023).

[25] T.-W. Su, L. Xue, and A. Ozcan, High-throughput lensfree 3D tracking of human sperms reveals rare statistics of helical trajectories, Proc. Natl. Acad. Sci. USA **109**, 16018 (2012).

[26] M. Qi, X. Gong, B. Wu, and G. Zhang, Landing dynamics of swimming bacteria on a polymeric surface: Effect of surface properties, Langmuir **33**, 3525 (2017).

[27] S. M. Mousavi, G. Gompper, and R. G. Winkler, Wall entrapment of peritrichous bacteria: A mesoscale hydrodynamics simulation study, Soft Matter **16**, 4866 (2020).

[28] The addition of polymer chains allows for systematic tuning of the angle θ, while leaving flagellar anchoring and bundling largely unaffected, as illustrated in Fig. 3(a). The increased fluid viscosity upon polymer addition also facilitates the visual inspection of precession and nutation (Fig. 2). Although one could simulate a population of bacteria with varying flagellar number and positioning to achieve different wobbling amplitudes, this approach is less efficient than adding polymer chains.

[29] See Supplemental Material at http://link.aps.org/supplemental/10.1103/g3w4-5jw8 for details, which includes Refs. [26,30–45].

[30] A. Malevanets and R. Kapral, Mesoscopic model for solvent dynamics, J. Chem. Phys. **110**, 8605 (1999).

[31] G. Gompper, T. Ihle, D. M. Kroll, and R. G. Winkler, Multi-particle collision dynamics: A particle-based mesoscale simulation approach to the hydrodynamics of complex fluids, Adv. Polym. Sci. **221**, 1 (2009).

[32] H. Noguchi and G. Gompper, Shape transitions of fluid vesicles and red blood cells in capillary flows, Proc. Natl. Acad. Sci. USA **102**, 14159 (2005).

[33] S. Sahoo, S. P. Singh, and S. Thakur, Role of viscoelasticity on the dynamics and aggregation of chemically active sphere-dimers, Phys. Fluids **33**, 017120 (2021).

[34] M. Chen, Z. Lin, M. Xuan, X. Lin, M. Yang, L. Dai, and Q. He, Programmable dynamic shapes with a swarm of light-powered colloidal motors, Angew. Chem. Intl. Ed. **60**, 16674 (2021).

[35] T. Li, Z. Liu, J. Hu, L. Chen, T. Chen, Q. Tang, B. Yu, B. Zhao, C. Mao, and M. Wan, A universal chemotactic targeted delivery strategy for inflammatory diseases, Adv. Mater. **34**, 2206654 (2022).

[36] H. Yamakawa, *Helical Wormlike Chains in Polymer Solutions* (Springer, Berlin, 1997).

[37] R. Vogel and H. Stark, Force-extension curves of bacterial flagella, Eur. Phys. J. E **33**, 259 (2010).

[38] P. J. A. Janssen and M. D. Graham, Coexistence of tight and loose bundled states in a model of bacterial flagellar dynamics, Phys. Rev. E **84**, 011910 (2011).

[39] S. Y. Reigh, R. G. Winkler, and G. Gompper, Synchronization and bundling of anchored bacterial flagella, Soft Matter **8**, 4363 (2012).

[40] R. M. Berry and H. C. Berg, Absence of a barrier to backwards rotation of the bacterial flagellar motor demonstrated with optical tweezers, Proc. Natl. Acad. Sci. USA **94**, 14433 (1997).

[41] M. Qi, Q. Song, J. Zhao, C. Ma, G. Zhang, and X. Gong, Three-dimensional bacterial behavior near dynamic surfaces formed by degradable polymers, Langmuir **33**, 13098 (2017).

[42] F. C. Cheong, B. J. Krishnatreya, and D. G. Grier, Strategies for three-dimensional particle tracking with holographic video microscopy, Opt. Express **18**, 13563 (2010).

[43] H. Goldstein, C. P. Poole, and J. L. Safko, *Classical Mechanics* (Pearson, Upper Saddle River, NJ, 2001), 3rd ed.

[44] C. Yang, C. Chen, Q. Ma, L. Wu, and T. Song, Dynamic model and motion mechanism of magnetotactic bacteria with two lateral flagellar bundles, J. Bionic Eng. **9**, 200 (2012).

[45] J. Lighthill, Flagellar hydrodynamics, SIAM Rev. **18**, 161 (1976).

[46] The overall rotation of the body is primarily due to precession, while the overall rotation of the flagellar bundle is dominated by spin. These two overall rotations are in opposite directions.

[47] The Python script and exemplary trajectory file for Euler angle analysis are available at https://doi.org/10.6084/m9.figshare.30121015.

[48] There are no such physical constraints in uniflagellated bacteria. The spin of body at a rate of about 30 Hz has been reported for *Caulobacter crescentus*, when the single flagellum pushes the cell forward [5].

[49] Our mesoscale hydrodynamics simulations that automatically include thermal fluctuations reveal that the time averages of the two instantaneous quantities, $\bar{L}_z$ and $\bar{L}_3$, are constants.

Correction: The equal contribution footnote for the first three authors was missing at publication and has been inserted.